minerals

MDPI

Article

Genesis of Calcite Veins in 8# Coal Seam of the Upper Carboniferous Benxi Formation, Southeastern Margin of Ordos Basin

Zheng Cao [1,2,3], Hairuo Qing [3,*], Cen Chen [1,2], Shijie Zhu [1,2], Xueying Lyu [1,2], Karem Azmy [4], Zhijun Li [1,2], Lei Zhang [1,2], Ruhao Liu [1,2] and Jiangen Xu [1,2]

[1] School of Petroleum Engineering, Chongqing University of Science and Technology, Chongqing 401331, China; caozheng_upc@126.com (Z.C.)
[2] Chongqing Key Laboratory of Complex Oil and Gas Exploration and Development, Chongqing University of Science and Technology, Chongqing 401331, China
[3] Department of Geology, University of Regina, Regina, SK S4S 0A2, Canada
[4] Department of Earth Sciences, Memorial University of Newfoundland, St. John's, NL A1B 3X5, Canada
* Correspondence: hairuo.qing@uregina.ca

Abstract: The 8# coal seam in the Benxi Formation of the southeastern margin of the Ordos Basin is a deep coal seam with abundant coalbed methane resources. Calcite veins are commonly developed within the 8# coal seam, and their formation processes and mechanisms have significant implications for the enrichment of deep coalbed methane. Genesis of the calcite veins was analyzed to reveal the impact of the calcite veins formation on coalbed methane accumulation, with an integrated application of petrographic study by thin section, cathodoluminescence analysis, carbon-oxygen isotope analysis, and homogeneous temperature measurements of fluid inclusions. The research findings indicate that the calcite veins in the 8# coal seam can be classified into three stages: C1, C2, and C3. The diagenetic fluids of C1 primarily originated from contemporaneous seawater. The fluids responsible for the formation of C2 primarily consist of organic fluids enriched in biogenic gas, whereas the fluids contributing to the formation of C3 are primarily associated with liquid hydrocarbons originated form decarboxylation of organic matter. Furthermore, the development of both C2 and C3 is influenced by deep hydrothermal fluids resulting from tectonic heating events during the Early Cretaceous. By combining analysis of the hydrocarbon accumulation history and burial history in the study area, it has been established that C2 formation occurred during the Late Triassic to Early Jurassic, while C3 formation took place during the Late Jurassic to Early Cretaceous. The exploration and production practices in the study area have firmly established the crucial significance of the formation and evolution of calcite veins within the 8# coal seam for the migration and accumulation of coalbed methane. The research outcomes provide valuable insights for the exploration of deep coalbed methane enrichment areas.

Keywords: calcite veins; petrographic study; C-O isotopes; fluid inclusion; deep coal seam; Ordos Basin

check for updates

Citation: Cao, Z.; Qing, H.; Chen, C.; Zhu, S.; Lyu, X.; Azmy, K.; Li, Z.; Zhang, L.; Liu, R.; Xu, J. Genesis of Calcite Veins in 8# Coal Seam of the Upper Carboniferous Benxi Formation, Southeastern Margin of Ordos Basin. *Minerals* **2023**, *13*, 879. https://doi.org/10.3390/min13070879

Academic Editors: Luis Miguel Nieto and José Miguel Molina

Received: 1 June 2023
Revised: 24 June 2023
Accepted: 27 June 2023
Published: 29 June 2023

Copyright: © 2023 by the authors. Licensee MDPI, Basel, Switzerland. This article is an open access article distributed under the terms and conditions of the Creative Commons Attribution (CC BY) license (https://creativecommons.org/licenses/by/4.0/).

1. Introduction

Fractures formed in coal seams under structural stress are one of the important channels for fluid activity and play an important role in controlling the migration and accumulation of coalbed methane [1,2]. During the fluid migration process, fluid-rock interactions occur with the surrounding rocks, leading to the formation of authigenic mineral filled fractures [3–14]. Therefore, conducting research on the authigenic mineral veins filling the fractures has important theoretical and practical significance in revealing fluid activity and coalbed methane accumulation processes [15–17]. Lithological observations, isotopic geochemistry, and fluid inclusion analysis are widely employed techniques for systematic research on the genesis mechanisms of authigenic mineral veins [18–23].

Currently, most of the developed coalbed methane blocks, both domestically and internationally, are situated at relatively shallow depths, primarily up to 1500 m [24,25]. However, in China, the latest assessment of coalbed methane resources has revealed a significant potential in deeper coal seams. Within the depth range from 1500 to 3000 m, China possesses a substantial volume of deep coalbed methane resources, estimated to be around 30×10^{12} m^3, accounting for a remarkable 54.5% of the total resources [26,27]. The 8# coal seam of the Upper Carboniferous Benxi Formation in the southeastern margin of the Ordos Basin represents a deep coalbed, with burial depths ranging from 1600 to 2800 m. The 8# coal seam is characterized by a well-developed fracture system and abundant coalbed methane resources, which has emerged as one of the key target layers for the exploration of deep coalbed methane resources in recent years.

Currently, the formation and evolution processes of calcite veins in the 8# coal seam of the Benxi Formation in the study area remain unclear, limiting in-depth knowledge of the enrichment laws of coalbed methane. In this study, a combination of thin section observations, cathodoluminescence analysis, carbon-oxygen isotope analysis, and homogeneous temperature measurements of fluid inclusions was employed to investigate the fluid sources and formation processes of calcite veins in the 8# coal seam of the Benxi Formation in the study area. The objective is to provide a solid foundation for enhancing our understanding of the enrichment patterns of coalbed methane in the 8# coal seam and to serve as a reference for studying the genesis of similar calcite veins in other similar basins.

2. Geological Setting

The Ordos Basin is a long-term and stable multi-cycle large craton superimposed basin with an area of 25×10^4 km^2. It consists of six secondary tectonic zones: the Yimeng uplift, Weibei uplift, Jinxi fold belt, Shanbei slope, Tianhuan depression, and western thrust belt [28]. The Daning-Jixian Block (the study area) is located in the southeastern Jinxi fold belt and is characterized by a gently dipping monoclinal with a NW dip and NNE trend (Figure 1).

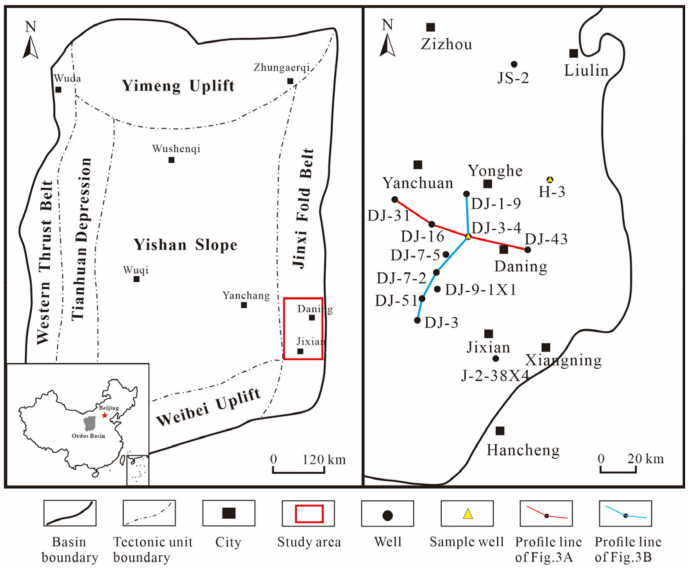


Figure 1. Map showing the location of the Ordos Basin and wells in the study area (modified from according to [29–31], revised).

The late Paleozoic coal-bearing strata in Ordos Basin are Carboniferous Benxi Formation, Permian Taiyuan, and Shanxi formations from bottom to top [32–34]. The Upper Carboniferous Benxi Formation in the study area was formed in coastal and shallow shelf environments [33]. Benxi Formation is divided into the first member (C_2b^1) and the second member (C_2b^2) from top to bottom. The C_2b^2 sediments are composed of bauxite and gray black mudstone with thin layers of sandy shale and limestone. The lithology of the C_2b^1 is

mainly gray medium and coarse quartz sandstone and dark gray coarse lithic sandstone, with mudstone and multiple sets of coal seams in the middle, and bioclastic limestone in the lower part (Figure 2). The 8# coal seam at the top of Benxi Formation is the main coal seam in this area, and the thickness is 3~10 m with buried depth of 1600~2800 m (Figure 3). The 8# coal seam is dominated by bright coal and penumbra coal with moderate metamorphism, which is one of the favorable strata for mid-rank coalbed methane enrichment in China and exhibits a good prospect of comprehensive exploration and development [32,34].

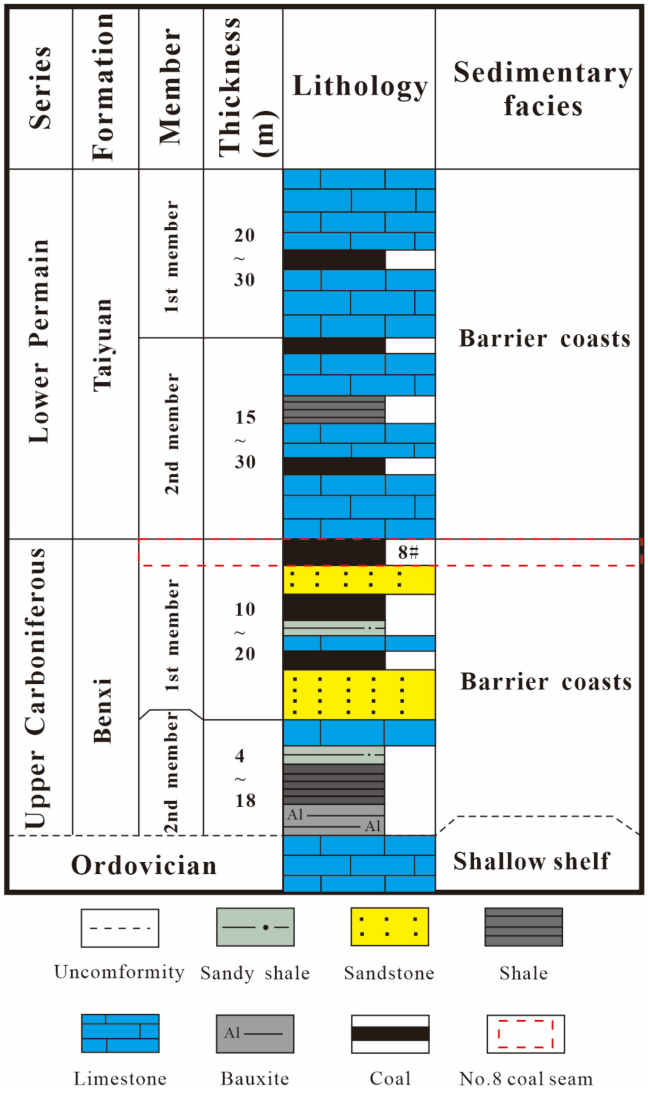


Figure 2. The stratigraphic column of the Upper Carboniferous Benxi Formation in the eastern margin of the Ordos Basin (according to [31], revised).

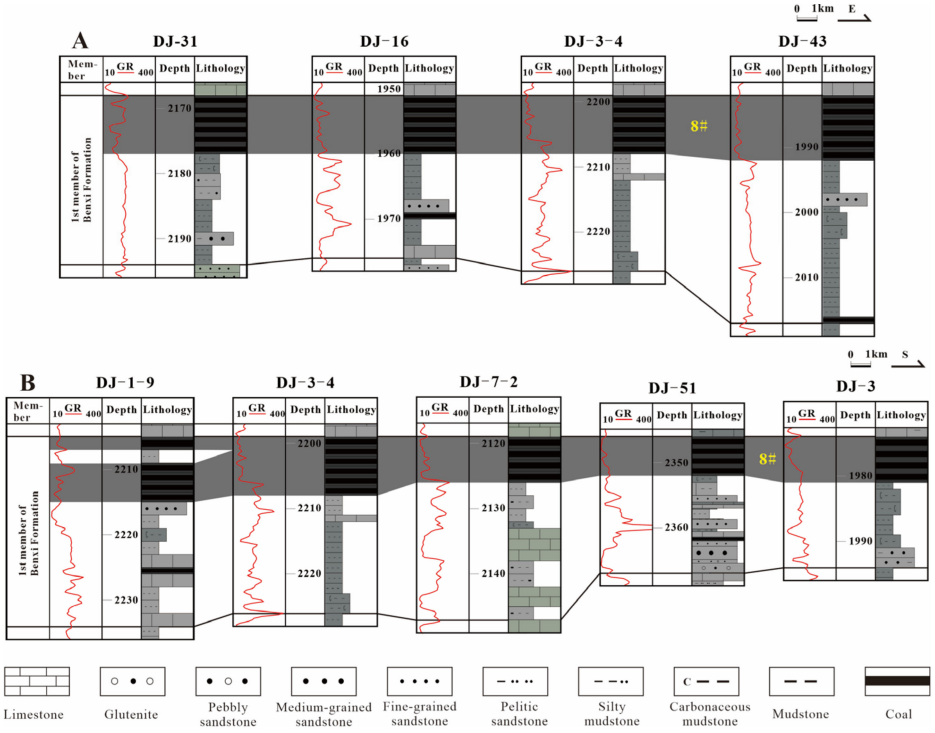


Figure 3. Stratigraphic profile showing distribution characteristics of the 8# coal seam. See Figure 1 for the profile locations of subfigures (**A**,**B**).

3. Materials and Methods

Five calcite vein samples were extracted from 8# coal seam of Benxi Formation within the depth interval of 2100~2300 m, Daning-Jixian block, southeastern margin of Ordos Basin, of which four samples were thin sectioned for petrographic analysis.

The petrography was studied on three coal samples containing calcite veins using a TESCAN-MIRA3 field emission scanning electron microscope (FESEM).

A total of four calcite veins double-polished sections (each ~100 µm) were prepared for fluid-inclusion analysis. Microthermometric measurements were conducted using a Linkam THMSG 600 heating-cooling stage, which offers a wide temperature range for phase transitions (−180 °C to 500 °C). The precision of the measured homogenization temperatures (T_h) is ±1 °C.

Four thin sections were examined using a Technosyn cold cathodoluminoscope at a current intensity of ~0.7 mA and an accelerating voltage of ~12 kV for cathodoluminescence (CL) observation.

Oxygen- and carbon-isotope analyses were conducted on five selected calcite vein samples. CO_2 was extracted from the powdered samples (50 mg each) by a reaction with 100% ultrapure orthophosphoric acid at 25 °C for 2 h in an inert atmosphere. The extracted CO_2 was analyzed for isotope ratios using a Thermo-Finnigan MAT 253 with the international standard NBS-18 ($\delta^{18}O$ = −23.0‰ and $\delta^{13}C$ = −5.01‰ vs. VPDB). The delta values ($\delta^{45/44}_{CO_2}$ and $\delta^{46/44}_{CO_2}$) were calibrated for ^{17}O effects [35] and adjusted for temperature-dependent kinetic oxygen isotope fractionation using a fractionation factor (α) of 1.01025 for calcite [36]. The results are reported in the per mil notation relative to the Vienna Pee Dee Belemnite (VPDB) standards. Uncertainties of the analyses are better than 0.15‰ (2σ), determined by repeated measurements of GBW04405 ($\delta^{13}C$ = +0.57‰ and $\delta^{18}O$ = −8.49‰ vs. VPDB) and GBW04406 ($\delta^{13}C$ = −10.85‰ and $\delta^{18}O$ = −12.40‰ vs. VPDB). $\delta^{18}O_{SMOW} = 1.03091 \times \delta^{18}O_{PDB} + 30.91$ [37].

4. Results

4.1. Petrography

High angle fractures of structure origin are common in the 8# coal seam in the study area. The fractures are developed in parallel and are commonly fulfilled with calcite. The width of a single calcite vein ranges from 0.5 mm to 1 mm, and the width of calcite veins fall in a range of 1~3 cm (Figure 4A–G). Calcite veins are observed to be parallel to or intersect with each other. Three stages of calcite in the calcite veins were identified in the 8# coal seam in the study area through thin sections and cathodoluminescence observation.

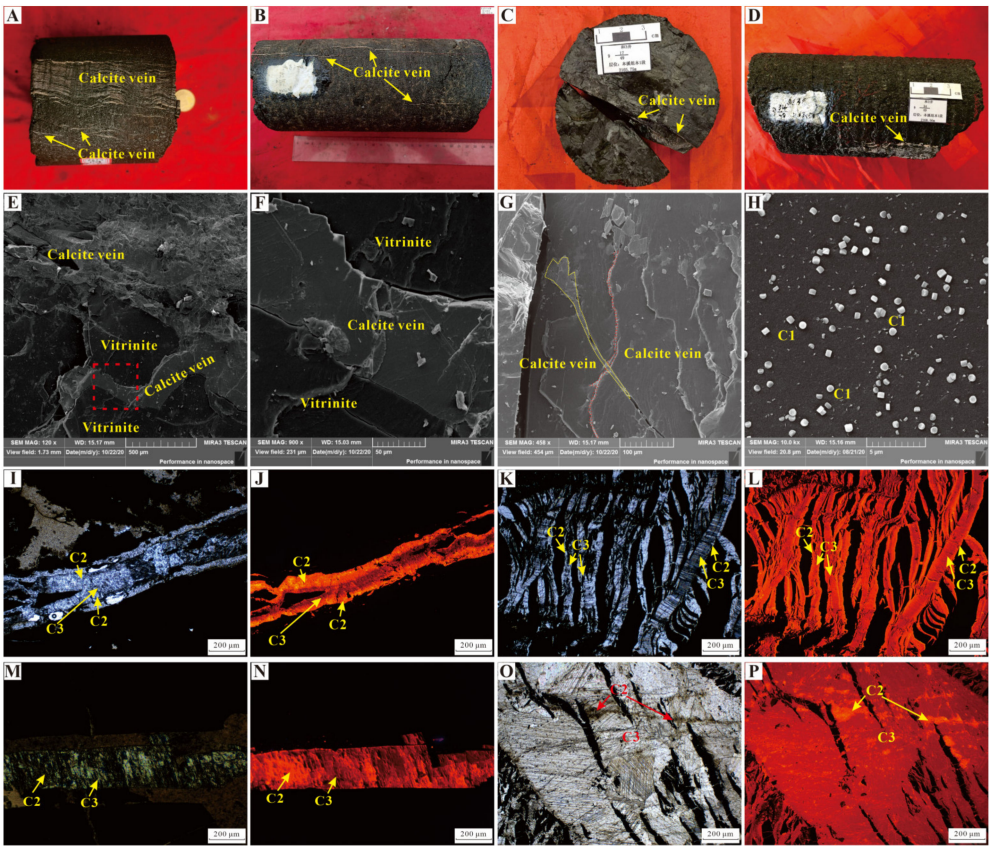


Figure 4. Petrographic characteristics of calcite veins in the 8# coal seam of the Benxi formation: (**A**) densely developed calcite veins (Well DJ-3-4, 2199.82 m); (**B**) structural origin high-angle fractures in coal filled with calcite (Well DJ-3-4, 2206.3 m); (**C**) structural origin high-angle fractures in coal filled with calcite (Well H-3, 2165.75 m); (**D**) densely developed calcite veins (Well H-3, 2168.56 m); (**E**) SEM image showing vitrinite and calcite veins, where calcite veins cross-cutting the vitrinite (Well H-3, 2168.5 m); (**F**) local enlargement (Figure (**M**), red dashed area), with calcite veins cutting through vitrinite (Well H-3, 2168.5 m); (**G**) SEM image showing calcite filled fractures, with the calcite vein on the left cutting through the right vein (Well H-3, 2168.5 m); (**H**) SEM image showing first-stage calcite developed on the surface of the vitrinite (Well DJ-3-4, 2203.2 m); (**I**) In XPL, C2 and C3 filled a single fracture (Well DJ-3-4, 2203.2 m); (**J**) Cathodoluminoscope image showing bright orange CL of the second-stage calcite and dark red CL of the third-stage calcite (Well DJ-3-4, 2203.2 m); (**K**) in XPL, C2 and C3 calcite filled the fractures (Well DJ-3-4, 2199.82 m); (**L**) Cathodoluminoscope image showing the third-stage calcite occupied a large amount of space in the fractures (Well DJ-3-4, 2199.82 m); (**M**) In XPL, C2 and C3 filled a single fracture (Well H-3, 2165.8 m); (**N**) Cathodoluminoscope image showing C2 and C3 filled fractures, where C3 replaced C2 (Well H-3, 2165.8 m); (**O**) In XPL, C2 and C3 filled the fractures (Well H-3, 2168.54 m); (**P**) Cathodoluminoscope image showing the third-stage calcite occupied a large amount of space in the fractures (Well H-3, 2168.54 m). XPL: cross-polarized light, C1: first-stage calcite; C2: second-stage calcite; C3: third-stage calcite.

The first stage of calcite (C1) is less developed, and commonly appears as microgranular on the surfaces of vitrinite (Figure 4H). The second-stage calcite (C2) predominantly consists of fine-grained calcite. It grows from both sides of the fracture walls towards the center, and exhibits a bright orange-red CL. The presence of significant dissolution features in C2 is apparent (Figure 4I–P). The third-stage calcite (C3) is characterized by medium to coarse-grained calcite and exhibits a dark red CL. It primarily develops in the residual space after the filling of C2 and is predominantly distributed in the middle of the fractures. It is evident that C3 replaces C2, and it can also completely fill the fractures (Figure 4I–P). The calcite veins in the 8# coal seam are primarily composed of C2 and C3. The differences in petrographic characteristics suggest that there may be variations in the fluid sources for the three stages of calcite.

4.2. Stable Isotopes of Calcite Veins

The $\delta^{13}C_{PDB}$ values of calcite veins fall in a wide range of −0.53‰~5.49‰, while the $\delta^{18}O_{SMOW}$ values vary from 18.14‰ to 19.88‰ (Table 1).

Table 1. Carbon and oxygen isotope composition of calcite veins in the 8# coal seam in the study area.

Well	Calcite Vein	Depth (m)	$\delta^{13}C_{PDB}$ (‰)	$\delta^{18}O_{PDB}$ (‰)	$\delta^{18}O_{SMOW}$ (‰)
DJ-3-4	C2	2206.30	5.49	−10.70	19.88
DJ-3-4	30%C2 + 70%C3	2199.82	0.44	−12.39	19.66
DJ-3-4	70%C2 + 30%C3	2203.20	4.82	−11.10	19.47
H-3	10%C2 + 90%C3	2168.56	−0.53	−11.98	18.56
H-3	60%C2 + 40%C3	2165.75	3.98	−10.91	18.14

The $\delta^{13}C_{PDB}$ values of the C2 are relatively high positive values, ranging from 3.98‰ to 5.49‰, while the $\delta^{18}O_{SMOW}$ values fall in a range of 18.14‰~19.88‰. The $\delta^{13}C_{PDB}$ values of the C3 are around 0‰, namely −0.53‰ and 0.44‰, while the $\delta^{18}O_{SMOW}$ range is 18.56‰ and −19.66‰ (Table 1).

4.3. Fluid Inclusions

The aqueous inclusions in calcite veins are randomly distributed and are mostly gas-liquid two-phase inclusions. The aqueous inclusions are colorless and transparent, mostly elliptical in shape, and range in size from about 3–16 μm (Figure 5).

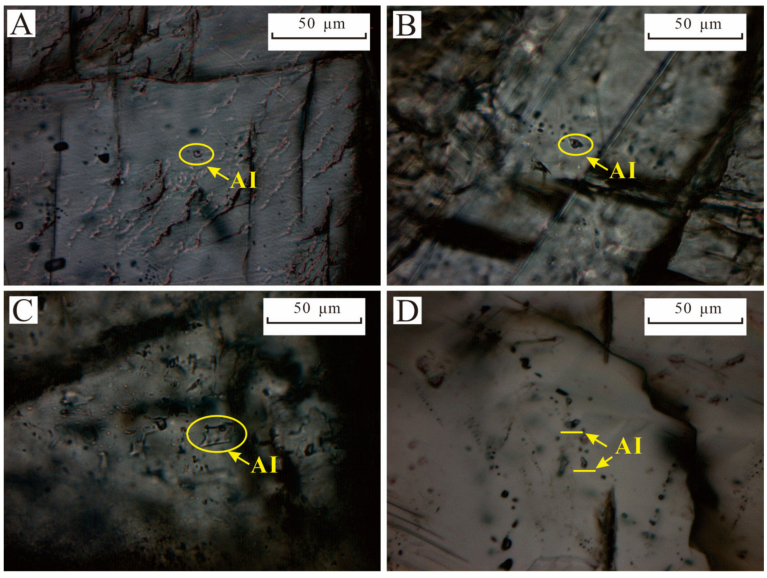


Figure 5. Photomicrographs showing two-phase aqueous inclusions in calcite: (**A**) C2, Well DJ-3-4, 2199.82 m; (**B**) C2, Well DJ-3-4, 2203.2 m; (**C**) C3, Well H-3, 2165.8 m; (**D**) C3, Well H-3, 2168.5 m. AI-aqueous inclusions.

The homogenization temperatures (T_h) values of the aqueous inclusions in the C2 range from 158 °C to 174 °C, with an estimated salinity of 19.68 to 22.03 wt.% NaCl equivalent. The T_h values of the aqueous inclusions in C3 are higher than those of C1, varying from 177 °C to 204 °C with a similar salinity range of 17.52 to 22.98 wt.% NaCl equivalent (Figure 6).

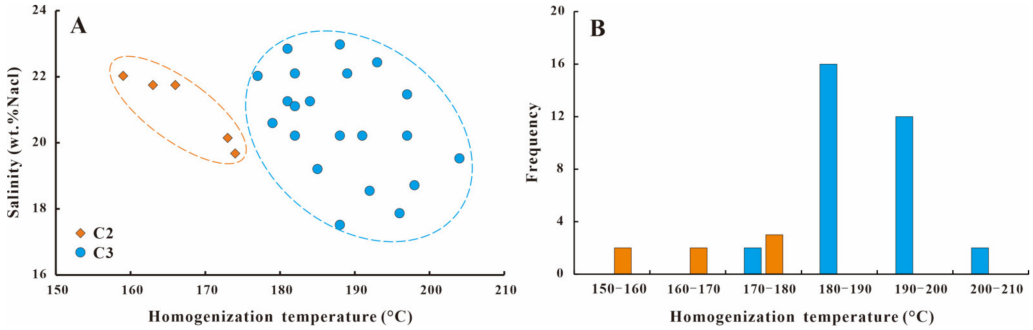


Figure 6. (**A**) Cross plot of homogenization temperature and salinity; (**B**) histograms showing homogenization temperatures for aqueous inclusions in calcite veins.

5. Discussion

5.1. Origin of Calcite Veins

The carbon and oxygen isotope composition of authigenic calcite can reflect the source and activity of diagenetic fluids during its formation [38–40]. Different carbon and oxygen isotopic reservoirs in nature exhibit significant variations [41,42]. For instance, the $\delta^{13}C_{PDB}$ values of the igneous carbonatite range from −8‰ to −4‰ and $\delta^{18}O_{SMOW}$ values from 6‰ to 10‰ [42], whereas marine carbonate show $\delta^{13}C_{PDB}$ values varying from −4‰ to 4‰ and $\delta^{18}O_{SMOW}$ values from 20‰ to 30‰ [41].

Thin section and SEM observations reveal that C1 is less common and primarily occurs as microcrystalline particles on the surfaces of vitrinite. This suggests that C1 may have formed during the syndepositional period, with diagenetic fluids predominantly consisting of contemporaneous seawater. The carbon and oxygen isotope compositions of C2 and C3 fall near the marine carbonate range (Figure 7A), indicating that the fluid sources of C2 and C3 may have partially originated from the dissolution of C1 formed during early diagenetic period.

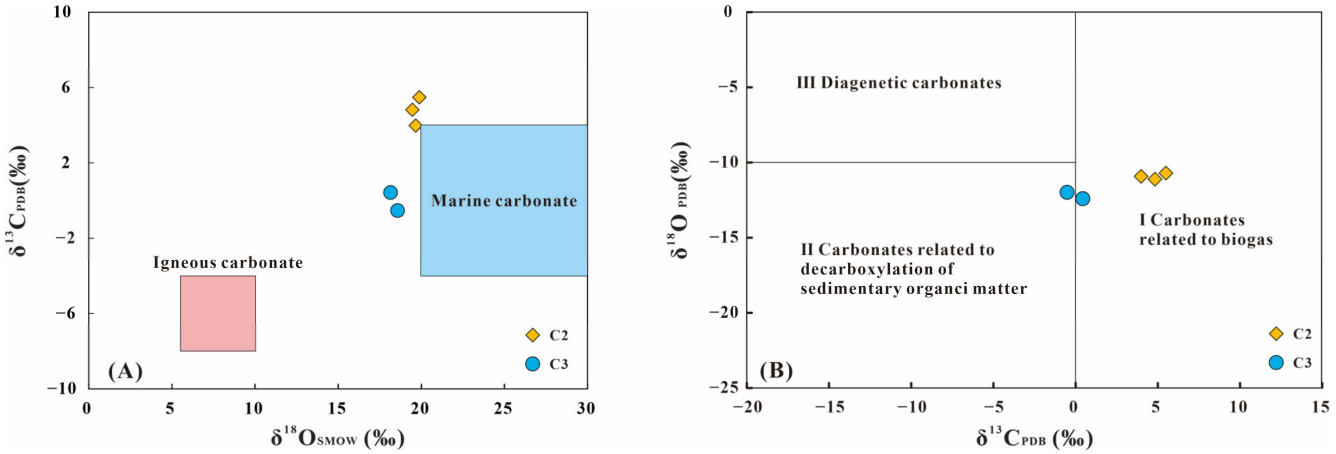


Figure 7. (**A**) Carbon and oxygen isotopic composition of the C2 and C3 in the calcite veins. Data of major geologic reservoirs are from [42,43]; (**B**) comprehensive identification of fluid source of calcite veins in the 8# coal seam (according to [44], revised).

The $\delta^{13}C$ and $\delta^{18}O$ values of the C2 range from 3.98‰ to 5.49‰ VPDB and from −11.10‰~−10.70‰ VPDB, respectively (Table 1). C2 exhibits characteristics of carbon

isotope enrichment and is located within the "carbonates related to biogenic gas" zone (Figure 7B). Organic matter typically undergoes processes such as oxidation, bacterial sulfate reduction, methane generation, and decarboxylation during burial evolution [45]. Carbonates formed through bacterial sulfate reduction display characteristics of depleted $\delta^{13}C$ and $\delta^{18}O$ (Figure 5b), while carbonates formed through methane production exhibit relatively enriched $\delta^{13}C$ values (0‰ < $\delta^{13}C$ < 15‰; Figure 5B). Therefore, the formation of C2 is related to methane bacterial reduction, with the diagenetic fluids mainly derived from organic fluids enriched in biogenic gas.

Compared to C2, the carbon isotope composition of C3 exhibits a relatively depleted feature and is located within the zone of carbonates related to decarboxylation of sedimentary organic matter (Figure 7B). The carbon isotope depletion may be related to the carbon source provided by the organic matter decarboxylation process in the oil generation window (−20‰ < $\delta^{13}C$ < 0‰), and the addition of organic carbon leads to the depletion of the diagenetic carbonates. Therefore, the primary source of diagenetic fluids for C3 is liquid hydrocarbons.

According to the study of the thermal and burial history of the Benxi Formation in the study area (Figure 8), it can be inferred that the maximum burial depth of the Benxi Formation is about 3500 m, corresponding to a paleotemperature of around 160 °C. However, the T_h ranges of the fluid inclusions in the C1 and C2 are 158–174 °C and 177–204 °C, respectively, both of which are higher than the maximum paleotemperature of the Benxi Formation. In addition, the observation and analysis of thin sections indicate that the two-stage calcite has undergone significant recrystallization, and the salinity of the fluid inclusions tested is relatively high. High-salinity fluids mostly originate from the deep basin [46,47]. The Ordos Basin has experienced strong magmatic activity in the Mesozoic and Cenozoic eras, including the Indosinian, Yanshanian, and Cenozoic volcanic activities, among which the late Yanshanian early Cretaceous volcanic activity in the Ordos Basin was the most intense [48–53]. Therefore, it is inferred that the 8# coal seam in the study area was injected with deep hydrothermal fluids during the Early Cretaceous.

Besides, peak temperature (T_{peak}) of the 8# coal seam for hydrothermal metamorphic setting is calculated according to Barker and Pawlewicz [54], and the equations are listed as below:

$$T_{peak} = (\ln(R_{v\text{-}r}) + 1.19)/0.00782 \text{ for hydrothermal metamorphism} \quad (1)$$

The vitrinite reflectance of the 8# coal seam is 1.49%~2.12% [34], and the mean random vitrinite reflectance ($R_{v\text{-}r}$) is adopted as 2.12%. The calculated result shows that the T_{peak} for hydrothermal metamorphism is 248 °C, which is higher than the maximum Th value (204 °C).

Based on this analysis, it is suggested that the 8# coal seam of the Benxi Formation in the study area underwent significant deep hydrothermal fluid influx during the Early Cretaceous. The presence of C2 and C3 with their respective fluid sources can be attributed to the intrusion of deep hydrothermal fluids associated with tectonic activities during the Yanshanian orogeny.

5.2. Formation Timing of Calcite Veins

Due to the influence of deep hydrothermal fluid intrusion caused by Early Cretaceous tectonic thermal events, the T_h of fluid inclusions in the calcite veins (C2 and C3) are higher than the formation temperature corresponding to the maximum burial depth of the strata. Therefore, it is not possible to determine the formation time of the two generations of calcite veins by the T_h of fluid inclusions and the thermal burial history of the strata.

The methane production of organic matter usually occurs during the shallow burial stage with temperatures below 75 °C, producing a certain amount of CO_2. As burial continues, when the temperature reaches 80–120 °C, organic matter will undergo decarboxylation to produce CO_2 and organic acids, entering the main stage of hydrocarbon generation. The accumulation period of the 8# coal seam of the Upper Carboniferous Benxi Formation in

the eastern Ordos Basin can be divided into two stages: the first stage is from the Early to Middle Jurassic, during which the coal-bearing source rocks reach the early maturity stage and begin to generate hydrocarbons; the second stage is from the Late Jurassic to Early Cretaceous, during which the liquid hydrocarbons formed earlier undergo thermal cracking to form gaseous hydrocarbons, marking the peak period of hydrocarbon generation and expulsion for the coal-bearing source rocks, i.e., the main accumulation period [49,50,52,53]. As mentioned earlier, the formation of the C2 is related to the methane production of organic matter (with temperatures below 75 °C), while the formation of the C3 is mainly related to decarboxylation of organic matter, and both are influenced by deep hydrothermal fluids. Combined with the thermal burial history of the study area, the temperature for methane production of organic matter is generally below 75 °C, corresponding to the Late Triassic period. Therefore, the C2 should have formed during the Late Triassic to Early Jurassic period, slightly earlier than the first stage of coalbed methane accumulation, while the formation of C3 is contemporaneous with the extensive hydrocarbon generation from organic matter and the occurrence of tectonic thermal events, corresponding to the second stage of coalbed methane accumulation during the Late Jurassic to Early Cretaceous (Figure 8).

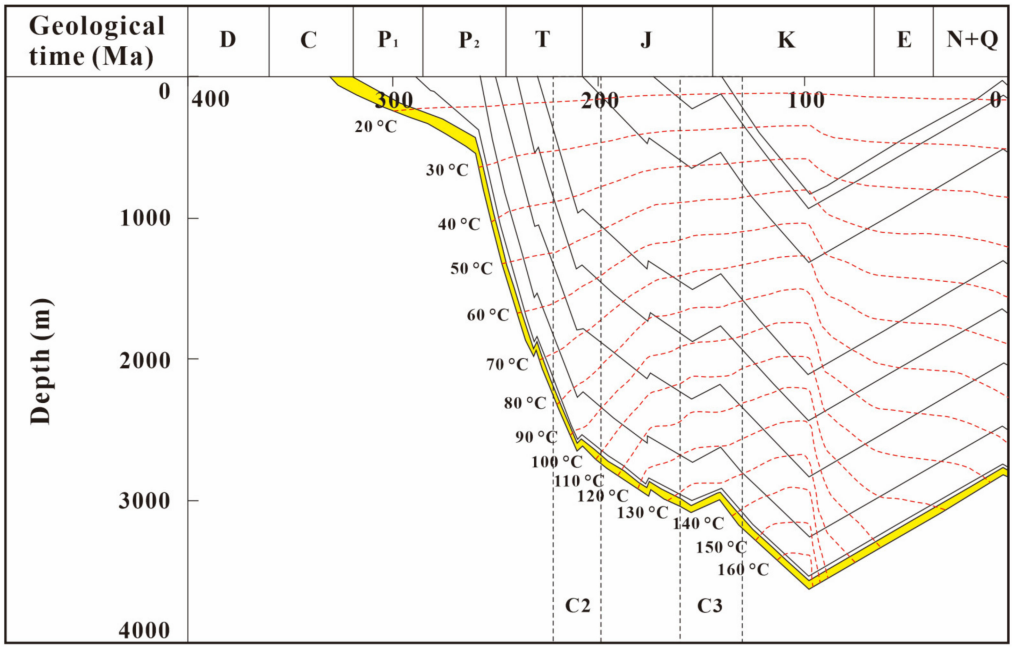


Figure 8. Burial and thermal history of the Carboniferous strata in the southeastern margin of the Ordos Basin (according to [55,56], revised).

In summary, the formation process of calcite veins in the 8# coal seam can be described as follows: During the early diagenetic stage, some mud-crystal calcite (C1) precipitated in the surrounding rocks and along the fracture edges. As the burial process progressed during the Late Triassic to Early Jurassic, the organic matter of the humic type underwent anaerobic bacterial fermentation, generating a significant amount of methane gas. The reduction of organic matter provided a carbon source for fluid-rock interactions, leading to the precipitation of calcite in association with Ca-bearing fluids from the surrounding rocks. The calcite filled the fractures, forming early stage calcite veins (C2). In the Late Jurassic to Early Cretaceous, influenced by the thermal evolution of organic matter, carbon-rich fluids with distinctive isotopic signatures acted as a carbon source. Late-stage calcite filled the remaining space in the fractures, exhibiting characteristics of carbon deficit. Concurrently, deep hydrothermal fluids infiltrated the area due to tectonic activities during the Yanshanian orogeny. These fluids caused dissolution and recrystallization of the late-stage calcite and some early stage calcite, giving rise to the third-stage calcite (C3; Figure 9).

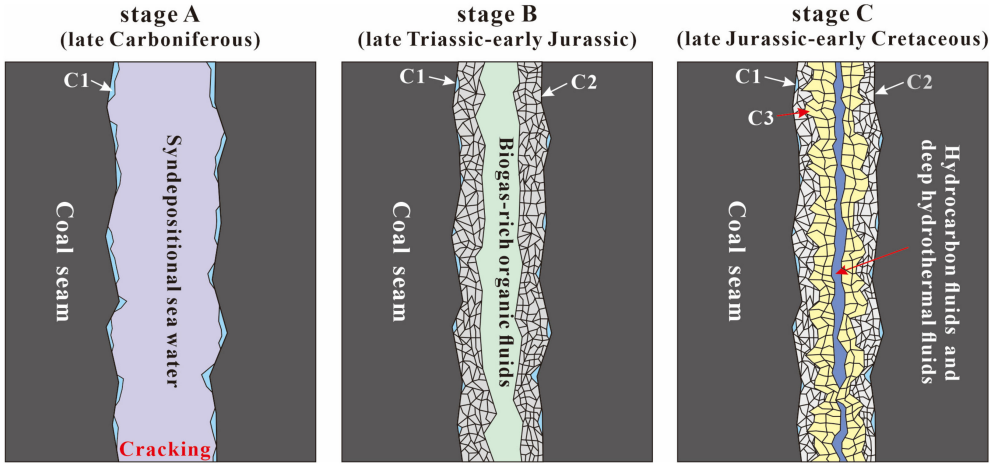


Figure 9. A schematic model for the formation of the calcite veins in the 8# coal seam. C1: light bule area; C2: grey area; C3: yellow area.

5.3. Implications on Coalbed Methane Exploration

The stress dispersion in the wide and gentle tectonic zone of the Daning-Jixian block on the eastern margin of the Ordos Basin has led to the development of fracture systems in the coal seam [49–53], and the time of large-scale fluid activity and the deposition and filling of calcite veins in coal seam fractures is contemporaneous.

The formation of C3 is contemporaneous with the extensive hydrocarbon generation from organic matter and the occurrence of tectonic thermal events, corresponding to the second period of coalbed methane accumulation (Late Jurassic to Early Cretaceous). On one hand, during this stage, the fractures were open [51–53], providing migration pathways for coalbed methane accumulation. On the other hand, the early influx of biogas-rich organic fluids and the later intrusion of hydrocarbon fluids led to the dissolution of C2, which improved the reservoir properties to some extent, thereby providing favorable conditions for coalbed methane accumulation and enrichment.

Recent exploration practices in the study area have also confirmed this understanding. The 8# coal seam in the study area is buried at a depth of around 2000 m, with daily gas production rates of 4387 m^3/d for DJ-7-5 well and 5574 m^3/d for DJ-9-1X1 well. In the south of the study area, the 8# coal seam in J-2-38X4 well is buried at a depth of around 1200 m, with a daily gas production rate of 4803 m^3/d. However, in the north of the study area, the JS-2 well, which is buried at a depth of around 900 m, has a daily gas production rate of only 810 m^3/d (Figure 10). Therefore, the development of calcite veins in the 8# coal seam in the study area is of great indicative significance for the coalbed methane enrichment zone.

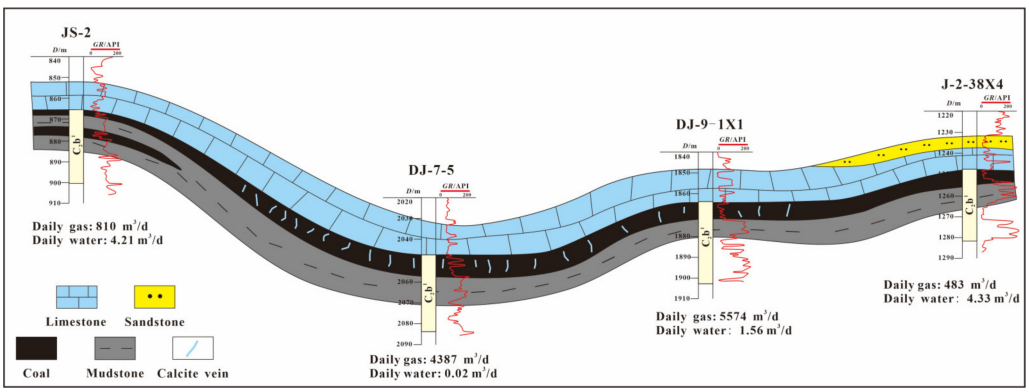


Figure 10. The accumulation profile of the 8# coal seam of the C_2b^1 unit in the study area.

6. Conclusions

Three stages of calcite are developed in the calcite veins of the 8# coal seam of the C_2b^1 in the study area. C1 is less developed, and commonly appears as microcrystalline particle on the surfaces of vitrinite The C2 predominantly consists of fine-grained calcite and grows from the edge of the fracture towards the center, showing a bright orange-red color under cathodoluminescence, with obvious dissolution. The C3 is characterized by medium to coarse-grained calcite and exhibits a dark red CL. The dissolution degree of C2 is weaker than that of C1. It primarily develops in the residual space after the filling of C2 and can also be observed completely filling the fractures.

The $\delta^{13}C_{PDB}$ values of C2 in the 8# coal seam range from 3.98‰ to 5.49‰, and the $\delta^{18}O_{SMOW}$ values vary from 18.14‰ to 19.88‰. The diagenetic fluids mainly origin from the formation of water of the surrounding rocks and organic fluids enriched in biogas. The $\delta^{13}C_{PDB}$ values of C3 range from −0.53‰ to 0.44‰, and the $\delta^{18}O_{SMOW}$ values vary from 18.56‰ to 19.66‰. The fluid source is mainly related to the liquid hydrocarbons formed by the decarboxylation of organic matter. At the same time, both C2 and C3 are affected by the deep hydrothermal fluids caused by the Early Cretaceous tectonic thermal event, resulting in higher temperatures of fluid inclusions both in C2 and C3.

The homogenization temperature distribution range of fluid inclusions in C2 is from 158 °C to 174 °C, formed during the Late Triassic-Early Jurassic period, slightly earlier than the first stage of coalbed methane accumulation. The homogenization temperature distribution of C3 is mainly distributed in the range of 177~204 °C, which corresponds to the second stage of coalbed methane accumulation, occurring during the Late Jurassic-Early Cretaceous period, when massive hydrocarbon generation and tectonic thermal events occurred.

The fractures hosting the calcite veins in the 8# coal seam of the Benxi Formation in the study area can provide migration pathways for the large-scale fluid activities associated with the formation of calcite veins (especially C3) during the main stage of coalbed methane accumulation. The areas with developed calcite veins exhibit a high degree of coalbed methane enrichment, indicating promising prospects for exploration and development.

Author Contributions: Conceptualization, Z.C.; Validation, S.Z., X.L. and J.X.; Resources, R.L.; Writing—original draft, Z.C.; Writing—review & editing, H.Q. and K.A.; Project administration, C.C., Z.L. and L.Z. All authors have read and agreed to the published version of the manuscript.

Funding: This research was co-funded by the National Natural Science Foundation of China (Grant No. 42102187), the Natural Science Foundation of Chongqing (Grant No. CSTB2022NSCQ-MSX1188), the Research Foundation of Chongqing University of Science and Technology (Grant No. ckrc2019040), and the Science and Technology Research Program of Chongqing Municipal Education Commission (No. KJQN202001518).

Data Availability Statement: Data will be made available on request.

Acknowledgments: We are grateful to the China United Coalbed Methane National Engineering Research Center Company Limited and PetroChina Coalbed Methane Company Limited, for providing data and for granting permission to publish the results.

Conflicts of Interest: The authors declare no conflict of interest.

References

1. Caja, M.A.; Permanyer, A.; Marfil, R.; Al-Aasm, I.S.; Martín-Crespo, T. Fluid flow record from fracture-fill calcite in the Eocene limestones from the South-Pyrenean Basin (NE Spain) and its relationship to oil shows. *J. Geochem. Explor.* **2006**, *89*, 27–32. [CrossRef]
2. Morad, S.; Al-Aasm, I.S.; Sirat, M.; Sattar, M.M. Vein calcite in cretaceous carbonate reservoirs of Abu Dhabi: Record of origin of fluids and diagenetic conditions. *J. Geochem. Explor.* **2010**, *106*, 156–170. [CrossRef]
3. Dawson, G.K.W.; Golding, S.D.; Esterle, J.S.; Massarotto, P. Occurrence of minerals within fractures and matrix of selected Bowen and Ruhr Basin coals. *Int. J. Coal Geol.* **2012**, *94*, 150–166. [CrossRef]

4. Diehl, S.F.; Goldhaber, M.B.; Koenig, A.E.; Lowers, H.A.; Ruppert, L.F. Distribution of arsenic, selenium, and other trace elements in high pyrite Appalachian coals: Evidence for multiple episodes of pyrite formation. *Int. J. Coal Geol.* **2012**, *94*, 238–249. [CrossRef]
5. Karayiğit, A.İ.; Mastalerz, M.; Oskay, R.G.; Buzkan, İ. Bituminous coal seams from underground mines in the Zonguldak Basin (NW Turkey): Insights from mineralogy, coal petrography, Rock-Eval pyrolysis, and meso-and microporosity. *Int. J. Coal Geol.* **2018**, *199*, 91–112. [CrossRef]
6. Permana, A.K.; Ward, C.R.; Li, Z.; Gurba, L.W. Distribution and origin of minerals in high-rank coals of the South Walker Creek area, Bowen Basin, Australia. *Int. J. Coal Geol.* **2013**, *116–117*, 185–207. [CrossRef]
7. Valentim, B.; Rodrigues, S.; Ribeiro, S.; Pereira, G.; Guedes, A.; Suárez-Ruiz, I. Relationships between the optical properties of coal macerals and the chars resulting from fluidized bed pyrolysis. *Int. J. Coal Geol.* **2013**, *111*, 80–89. [CrossRef]
8. Xie, P.; Hower, J.C.; Liu, X. Petrographic characteristics of the brecciated coals from Panxian county, Guizhou, southwestern China. *Fuel* **2019**, *243*, 1–9. [CrossRef]
9. Guo, K.; Zeng, J.; Li, Y.; Liu, T. Geochemical characteristics of tectonic fracture-filling calcite in Yanchang formation of Longdong area and its relationship with hydrocarbon fluid flow. *J. China Univ. Pet.* **2013**, *37*, 36–42.
10. Wang, R.Y.; Ding, W.L.; Gong, D.J.; Zeng, W.T.; Wang, X.H.; Zhou, X.H.; Li, A.; Xiao, Z.K. Development characteristics and major controlling factors of shale fractures in the Lower Cambrian Niutitang Formation, southeastern Chongqing-northern Guizhou area. *Acta Pet. Sin.* **2016**, *37*, 832–845.
11. Wang, R.; Ding, W.; Zhang, Y.; Wang, Z.; Wang, X.; He, J.; Zeng, W.; Dai, P. Analysis of developmental characteristics and dominant factors of fractures in Lower Cambrian marine shale reservoirs: A case study of Niutitang formation in Cen'gong block, southern China. *J. Pet. Sci. Eng.* **2016**, *138*, 31–49. [CrossRef]
12. Wang, R.Y.; Hu, Z.Q.; Zhou, T.; Bao, H.Y.; Wu, J.; Du, W.; He, J.H.; Wang, P.W.; Chen, Q. Characteristics of fractures and their significance for reservoirs in Wufeng-Longmaxi shale, Sichuan Basin and its periphery. *Oil Gas Geol.* **2021**, *42*, 1295–1306.
13. Sun, Y.; Ju, Y.; Zhou, W.; Qiao, P.; Tao, L.; Xiao, L. Nanoscale pore and crack evolution in shear thin layers of shales and the shale gas reservoir effect. *Adv. Geo-Energy Res.* **2022**, *6*, 221–229. [CrossRef]
14. Jiang, W.P.; Zhang, P.H.; Li, D.D.; Li, Z.C.; Wang, J.; Duan, Y.N.; Wu, J.; Liu, N.N. Reservoir characteristics and gas production potential of deep coalbed methane: Insights from the no. 15 coal seam in shouyang block, Qinshui Basin, China. *Unconv. Resour.* **2022**, *2*, 12–20. [CrossRef]
15. Gao, G.; Elmore, R.D.; Land, L.S. Geochemical constraints on the origin of calcite veins and associated limestone alteration, Ordovician Viola Group, Arbuckle Mountains, Oklahoma, USA. *Chem. Geol.* **1992**, *98*, 257–269. [CrossRef]
16. Lander, R.H.; Larese, R.E.; Bonnell, L.M. Toward more accurate quartz cement models: The importance of euhedral versus noneuhedral growth rates. *AAPG Bull.* **2008**, *92*, 1537–1563. [CrossRef]
17. Worden, R.H.; Benshatwan, M.S.; Potts, G.J.; Elgarmadi, S.M. Basin-scale fluid movement patterns revealed by veins: Wessex Basin, UK. *Geofluids* **2016**, *16*, 149–174. [CrossRef]
18. Jochum, J.; Friedrich, G.; Leythaeuser, D.; Littke, R.; Ropertz, B. Hydrocarbon-bearing fluid inclusions in calcite-filled horizontal fractures from mature Posidonia Shale (Hils Syncline, NW Germany). *Ore Geol. Rev.* **1995**, *9*, 363–370. [CrossRef]
19. Suchý, V.; Dobeš, P.; Sýkorová, I.; Machovič, V.; Stejskal, M.; Kroufek, J.; Chudoba, J.; Matějovský, L.; Havelcová, M.; Matysová, P. Oil-bearing inclusions in vein quartz and calcite and, bitumens in veins: Testament to multiple phases of hydrocarbon migration in the Barrandian basin (lower Palaeozoic), Czech Republic. *Mar. Pet. Geol.* **2010**, *27*, 285–297. [CrossRef]
20. Nothdurft, L.D.; Webb, G.E.; Kamber, B.S. Rare earth element geochemistry of Late Devonian reefal carbonates, Canning Basin, Western Australia: Confirmation of a seawater REE proxy in ancient limestones. *Geochim. Cosmochim. Acta* **2004**, *68*, 263–283. [CrossRef]
21. Guo, X.; Liu, K.; Jia, C.; Song, Y.; Zhao, M.; Zhuo, Q.; Lu, X. Fluid evolution in the Dabei Gas Field of the Kuqa Depression, Tarim Basin, NW China: Implications for fault-related fluid flow. *Mar. Pet. Geol.* **2016**, *78*, 1–16. [CrossRef]
22. Roberts, N.M.; Rasbury, E.T.; Parrish, R.R.; Smith, C.J.; Horstwood, M.S.; Condon, D.J. A calcite reference material for LA-ICP-MS U-Pb geochronology. *Geochem. Geophys. Geosystems* **2017**, *18*, 2807–2814. [CrossRef]
23. Roberts, N.M.; Holdsworth, R.E. Timescales of faulting through calcite geochronology: A review. *J. Struct. Geol.* **2022**, *158*, 104578. [CrossRef]
24. Liu, D.; Qiu, F.; Liu, N.; Cai, Y.; Guo, Y.; Zhao, B.; Qiu, Y. Pore structure characterization and its significance for gas adsorption in coals: A comprehensive review. *Unconv. Resour.* **2022**, *2*, 139–157. [CrossRef]
25. Zeng, W.T.; Ge, T.Z.; Wang, Q.; Pang, B.; Liu, Y.H.; Zhang, K.; Yu, L.Z. Exploration of integrated technology for deep coalbed methane drainage in full life cycle: A case study of Daning–Jixian Block. *Coal Geol. Explor.* **2022**, *50*, 78–85.
26. Xu, F.Y.; Yan, X.; Li, S.G.; Xiong, X.Y.; Wang, Y.X.; Zhang, L.; Liu, C.Q.; Han, J.L.; Feng, Y.Q.; Zhen, H.B.; et al. Theoretical and technological difficulties and countermeasures of deep CBM exploration and development in the eastern edge of Ordos Basin. *Coal Geol. Explor.* **2023**, *51*, 115–130.
27. Kang, Y.S.; Huangpu, Y.H.; Zhang, B.; Deng, Z.; Mao, D.L.; He, Z.P.; Wang, J.; Yuan, C.L. Formation conditions for deep oversaturated coalbed methane in coal-bearing basins. *Acta Pet. Sin.* **2019**, *40*, 1426.
28. Jia, L.B.; Zhong, D.K.; Ji, Y.L.; Zhou, Y.; Liu, J.L.; Mi, L.J.; Li, D.J.; Yan, R.T.; Yi, Z.; Jia, L.K. Architecture of tectonic sequences, depositional systems, and tectonic controls of the sedimentary fills of the rift-related Wenchang Formation in the Lufeng Depression, Pearl River Mouth Basin, China. *Geol. J.* **2019**, *54*, 1950–1975. [CrossRef]

29. Cao, Z.; Lin, C.Y.; Dong, C.M.; Ren, L.H.; Han, S.; Dai, J.J.; Xu, X.; Qin, M.Y.; Zhu, P. Impact of sequence stratigraphy, sedimentary facies, diagenesis and CO_2 charge on reservoir quality of the lower cretaceous Quantou Formation, Southern Songliao Basin, China. *Mar. Pet. Geol.* **2018**, *93*, 497–519. [CrossRef]
30. Cao, Z.; Azmy, K.; Lin, C.; Dong, C.; Ren, L.; Qin, M.; Li, Z.J.; Tan, X.F.; Zhang, L.; Li, X.G. Diagenetic evolution of the lower Yaojia Formation of Songliao Basin, China: Impact on reservoir quality. *J. Pet. Sci. Eng.* **2022**, *213*, 110415. [CrossRef]
31. Kuang, L.C.; Dong, D.Z.; He, W.Y.; Wen, S.M.; Sun, S.S.; Li, S.X.; Qiu, Z.; Liao, X.W.; Li, Y.; Wu, J.; et al. Geological characteristics and development potential of transitional shale gas in the east margin of the Ordos Basin, NW China. *Pet. Explor. Dev.* **2020**, *47*, 435–446. [CrossRef]
32. Sun, B.; Wang, X.H.; Chen, C.H.; Zhang, J.D. Distribution characteristics of the coalbed methane at Daning–Jixian region in Ordos Basin. *Nat. Gas Ind.* **2004**, *24*, 17–20.
33. Sun, Q.P.; Wang, S.W. The deposit environment analysis of the coal-bearing strata and its significance to the coalbed methane development in Daning-Jixian region. *Nat. Gas Geosci.* **2006**, *17*, 874–879.
34. Li, W.Z.; Chen, G.; Sun, B.; Sun, F.J.; Zhao, Q.B. Geological controls of coalbed methane enrichment in Daning-Jixian area, southeastern Ordos Basin. *Nat. Gas Geosci.* **2011**, *22*, 352–360.
35. Craig, H. Isotopic standards for carbon and oxygen and correction factors for mass-spectrometric analysis of carbon dioxide. *Geochim. Cosmochim. Acta* **1957**, *12*, 133–149. [CrossRef]
36. Sharma, T.; Clayton, R.N. Measurement of $O^{18}O^{16}$ ratios of total oxygen of carbonates. *Geochim. Cosmochim. Acta* **1965**, *29*, 1347–1353. [CrossRef]
37. Coplen, T.B.; Kendall, C.; Hopple, J. Comparison of stable isotope reference samples. *Nature* **1983**, *302*, 236–238. [CrossRef]
38. Elburg, M.A.; Bons, P.D.; Foden, J.; Passchier, C.W. The origin of fibrous veins: Constraints from geochemistry. *Geol. Soc. Lond. Spec. Publ.* **2002**, *200*, 103–118. [CrossRef]
39. Machel, H.G. Fibrous gypsum and fibrous anhydrite in veins. *Sedimentology* **2010**, *32*, 443–454. [CrossRef]
40. Hilgers, C.; Sindern, S. Textural and isotopic evidence on the fluid source and transport mechanism of antitaxial fibrous micro-structures form the Alps and the Appalachians. *Geofluids* **2010**, *5*, 239–250. [CrossRef]
41. Veizer, J.; Hoefs, J. The nature of O^{18}/O^{16} and C^{13}/C^{12} secular trends in sedimentary carbonate rocks. *Geochim. Cosmochim. Acta* **1976**, *40*, 1387–1395. [CrossRef]
42. Demény, A.; Ahijado, A.; Casillas, R.; Vennemann, T.W. Crustal contamination and fluid/rock interaction in the carbonatites of Fuerteventura (Canary Islands, Spain): A C, O, H isotope study. *Lithos* **1998**, *44*, 101–115. [CrossRef]
43. Hoefs, J. *Stable Isotope Geochemistry*, 6th ed.; Springer: Berlin/Heidelberg, Germany; New York, NY, USA; London, UK; Paris, France; Tokyo, Japan, 2009; 286p.
44. Wang, D.R. *The Oil Gas Stabilizes Isotope Geochemistry*; Petroleum Industry Press: Beijing, China, 2000; pp. 179–183. (In Chinese)
45. Irwin, H.; Curtis, C.; Coleman, M. Isotopic evidence for source of diagenetic carbonates formed during burial of organic-rich sediments. *Nature* **1977**, *269*, 209–213. [CrossRef]
46. Goldstein, R.H. Fluid inclusions in sedimentary and diagenetic systems. *Lithos* **2001**, *55*, 159–193. [CrossRef]
47. Fischer, M.P.; Higuera-Díaz, I.C.; Evans, M.A.; Perry, E.C.; Lefticariu, L. Fracture-controlled paleohydrology in a map-scale detachment fold: Insights from the analysis of fluid inclusions in calcite and quartz veins. *J. Struct. Geol.* **2009**, *31*, 1490–1510. [CrossRef]
48. Ren, Z.L. Application of apatite fission-track analysis method to the study of thermal history of the Ordos Basin. *Chin. J. Geophys.* **1995**, *38*, 339–349.
49. Sun, S.H.; Li, X.M.; Gong, G.L.; Liu, S.S. Study on tectonic thermal events in the Ordos Basin. *Chin. Sci. Bull.* **1997**, *42*, 306–309.
50. Chen, R.Y.; Luo, X.R.; Zhao, W.Z.; Wang, H.J. Thermal anomaly and thermal evolution of source rocks in Mesozoic, Ordos Basin. *Pet. Explor. Dev.* **2007**, *34*, 658–663.
51. Ren, Z.L.; Zhang, S.; Gao, S.L.; Cui, J.P.; Liu, X.S. Research on region of maturation anomaly and formation time in Ordos Basin. *Acta Geol. Sin.* **2006**, *80*, 674–684.
52. Ren, Z.L.; Zhang, S.; Gao, S.L.; Cui, J.P.; Xiao, Y.Y.; Xiao, H. Tectonic thermal history and its significance on the formation of oil and gas accumulation and mineral deposit in Ordos Basin. *Sci. China Ser. D Earth Sci.* **2007**, *50*, 27–38. [CrossRef]
53. Ren, Z.L.; Cui, J.P.; Qi, K.; Yang, G.L.; Chen, Z.J.; Yang, P.; Wang, K. The control of deep and ultra deep temperature and thermal evolution history on oil and gas facies and hydrocarbon generation history. *Nat. Gas Ind.* **2020**, *40*, 22–29.
54. Barker, C.E.; Pawlewicz, M.J. Calculationofvitrinitereflectance from thermal histories and peak temperatures: A comparison of methods. In *Vitrinite Reflectance as a Maturity Parameter, American Chemical Society Symposium Series*; Mukhopadhyay, P.K., Dow, W.G., Eds.; American Chemical Society: Washington, DC, USA, 1994; Volume 570, pp. 216–229.
55. Zhao, D.F.; Zhao, J.Z.; Chen, Y. An analysis on the characteristics of the Shan-2 formation gas pools in Yulin-Zizhou area of Ordos basin. *Nat. Gas Geosci.* **2013**, *24*, 320–328.
56. Fan, W.T.; Hu, G.H.; Wang, T. A simulation of thermal evolution history in southern margin of Ordos basin. *China Sci. Pap.* **2019**, *14*, 492–496.

Disclaimer/Publisher's Note: The statements, opinions and data contained in all publications are solely those of the individual author(s) and contributor(s) and not of MDPI and/or the editor(s). MDPI and/or the editor(s) disclaim responsibility for any injury to people or property resulting from any ideas, methods, instructions or products referred to in the content.